Article

Yield Predictions of Four Hybrids of Maize (*Zea mays*) Using Multispectral Images Obtained from UAV in the Coast of Peru

David Saravia [1,2], Wilian Salazar [1], Lamberto Valqui-Valqui [1], Javier Quille-Mamani [1,3], Rossana Porras-Jorge [1,2], Flor-Anita Corredor [1], Elgar Barboza [1,4], Héctor V. Vásquez [1,4], Andrés V. Casas Diaz [2] and Carlos I. Arbizu [1,*]

1   Dirección de Desarrollo Tecnológico Agrario, Instituto Nacional de Innovación Agraria (INIA), Av. La Molina, 1981, Lima 15024, Peru
2   Facultad de Agronomía, Universidad Nacional Agraria La Molina, Av. La Molina s/n, Lima 15024, Peru
3   Grupo de Cartografía GeoAmbiental y Teledetección, Universitat Politècnica de València, Camí de Vera s/n, 46022 Valencia, Spain
4   Instituto de Investigación para el Desarrollo Sustentable de Ceja de Selva (INDES-CES), Universidad Nacional Toribio Rodríguez de Mendoza de Amazonas (UNTRM), Chachapoyas 01001, Peru
*   Correspondence: carbizu@inia.gob.pe; Tel.: +51-986-288-181

Abstract: Early assessment of crop development is a key aspect of precision agriculture. Shortening the time of response before a deficit of irrigation, nutrients and damage by diseases is one of the usual concerns in agriculture. Early prediction of crop yields can increase profitability for the farmer's economy. In this study, we aimed to predict the yield of four maize commercial hybrids (Dekalb7508, Advanta9313, MH_INIA619 and Exp_05PMLM) using vegetation indices (VIs). A total of 10 VIs (NDVI, GNDVI, GCI, RVI, NDRE, CIRE, CVI, MCARI, SAVI, and CCCI) were considered for evaluating crop yield and plant cover at 31, 39, 42, 46 and 51 days after sowing (DAS). A multivariate analysis was applied using principal component analysis (PCA), linear regression, and r-Pearson correlation. Highly significant correlations were found between plant cover with VIs at 46 (GNDVI, GCI, RVI, NDRE, CIRE and CCCI) and 51 DAS (GNDVI, GCI, NDRE, CIRE, CVI, MCARI and CCCI). The PCA showed clear discrimination of the dates evaluated with VIs at 31, 39 and 51 DAS. The inclusion of the CIRE and NDRE in the prediction model contributed to estimating the performance, showing greater precision at 51 DAS. The use of unmanned aerial vehicles (UAVs) to monitor crops allows us to optimize resources and helps in making timely decisions in agriculture in Peru.

Keywords: vegetation indices; precision farming; hybrid; phenotyping; remote sensing

1. Introduction

World population growth is constant over time, with estimates of 9.7 billion people by 2050 and 11 billion by 2100 [1]. Therefore, it is imperative to strengthen food security and increase crop production through the efficient use of resources for its sustainability. In this sense, maize is one of the most important cereals in the world and a staple food in many households. It is also a source of animal feed and a fundamental product in the food industry [2,3]. World production is estimated at 1192 Mt, with the largest producers being the United States, China, Brazil and Mexico [4].

In the last decade, the use of technologies in agriculture has also increased significantly through the usage of Geographic Information Systems (GIS), Global Navigation Satellite Systems (GNSS), remote sensing, UAVs, machinery and other technologies that have supported precision agriculture [5–7]. The incorporation of these disciplines allows the collection, processing and analysis of temporal, spatial and individual data, and combines them with other data for the implementation of adequate solutions in the use of resources, productivity, quality, profitability and sustainability of agricultural production [8–11].

A wide range of UAVs and satellite-mounted sensors have been used for phenotyping studies to obtain aerial images and monitor crop development [12,13]. Landsat and Sentinel-2 satellites collect images in the visible and near-infrared (NIR) to assess the health of crop development on a regional and global scale [14–17]. However, the spatial resolution has not been fine enough to meet the phenotypic measurement needs of various research projects on crops and in small areas at the level of small agricultural producers [12,18]. For this reason, the use of UAVs is currently gaining prestige as an integral part of precision agriculture or agriculture 4.0, guaranteeing successful harvests [19].

On the other hand, UAVs with remote sensors can collect detailed information on the phenological development of crops through high spatial and temporal resolution images, which greatly reduces labor and time costs [20–22]. These sensors can acquire bands such as thermal infrared, RGB band, NIR band and red edge (RE) band [19]. These bands allow studying biomass growth, nitrogen content, yield, water stress and chlorophyll measurement in citrus, maize, wheat, soybean and grapevine crops [11,22–27], through the application of VIs such as the normalized difference vegetation index (NDVI) and other indices based on reflectance [12].

Accurate estimation of maize yield at the local or regional level contributes to improved food security and the development of more supportive models. [28]. In Peru, the cultivated area of yellow dent maize during the 2019–2020 season was 237,000 hectares with a production of 5.0 Mt per hectare (siea.midagri.gob.pe/portal/siea_bi/index.html, accessed on 11 June 2022). However, in recent years these varieties have become very susceptible to new climate change conditions [29], making real-time crop monitoring and supervision very useful in Peru. There is also limited availability of technologies to facilitate crop detection, monitoring and analysis as these techniques are in their infancy in Peru. In this context, the use of UAVs and multispectral sensors are an excellent option to evaluate and estimate corn production [30], allowing us to prevent crop damage and increase farmers' economies. Consequently, in this study we evaluated the performance of four maize hybrids on the Peruvian coast, calculating VIs from multispectral images obtained from UAVs.

2. Materials and Methods

2.1. Study Area

The data collection was carried out at the Centro Experimental La Molina (CELM) of the Instituto Nacional de Innovación Agraria (INIA) ($-12°4'$ W, $-76°56'$ S) which is located in the district of La Molina, province and department of Lima (Peru), Figure 1.

This area is characterized by a semi-arid climate, presenting an annual rainfall of 5.7 mm year^{-1} and an average temperature of 17.3 °C in 2021 (CELM Automatic Weather Station, VANTAGE Pro2 Plus Davis, CA, USA). The type of soil is sandy loam with physical characteristics of electrical conductivity (EC) of 1.59 dS/m, pH of 7.32, field capacity of 14.8%, wilting point of 7.7% and bulk density of 1.54 g/cm^3 (INIA-Water, Soil and Foliar Research Laboratory).

The experimental field consisted of 48 plots with four commercial maize hybrids (Dekalb7508, Advanta9313, MH_INIA619 and Exp_05PMLM). They have a vegetative period of approximately 120 days and adapt very well to different regions of the Peruvian coast. Each plot represented an area of 32.8 m^2 (8 m long and 4.1 m wide) with five furrows spaced 0.9 m apart and between plant bumps at 0.25 m. The season of greater planting of the crop is carried out in spring-summer. The evaluation and monitoring of the field experiment began with sowing on 18 January 2021, to end with its harvest on May 31 of the same year. During the vegetative period, the maximum temperature recorded was 30.4 °C in January, while the minimum was 15 °C in June.

A drip irrigation system was used, with a drip flow rate of 3.7 L/h and a distance between drippers of 0.2 m. Management practices such as weed and pest control were carried out manually and the use of herbicides was part of the agronomic management of the field.

Figure 1. Location of the study area the La Molina Experimental Center in Lima (Peru).

2.2. Data Collection

Yield grain data was obtained by manually harvesting the ears from a representative area of 32.8 m^2 in each plot and then expressed as t/ha. The process consisted of weighting the total maize grains of each plot with 20–25% humidity, and then extracting a 200 g sample per plot to be dried in an oven at 60 °C for an interval of 72 h, reaching grain moisture of approximately 12–14% to estimate yield per hectare.

Images obtained from the UAV Phantom 4 Pro (https://www.dji.com/phantom-4-pro?site=brandsite&from=nav, Shenzhen, China, accessed on 22 March 2022) covered the different stages of maize development. They were collected between 11:00 a.m. and 2:00 p.m. to minimize changes in the solar zenith angle in cloudless weather conditions [31]. Five dates were selected for the acquisition of the images (31, 39, 42, 46 and 51 DAS) between January and March 2021. The selection of the dates for the acquisition of the images was made considering the previous stages of flowering and the maximum coverage of the maize canopy. At these stages, the VIs reached their highest levels and then went down. The UAV coupled with Parrot Sequoia multispectral camera (Parrot SA, Paris, France) (Figure 2) was used to acquire the images of the 48 study units at a height of 30 m.

The focal length of the camera was 5 mm with an image shutter speed of 1 s. Each image was composed of four bands in the wavelength ranges from 530 to 570 nm (Green); 640 to 680 nm (Red); 730 to 740 nm (Red edge); 770 to 810 nm (Near-Infrared), with a spatial resolution of 1.2 megapixels [32], and the image size was 1280 × 960 pixels. The files were saved in the Tagged Image File Format (TIFF).

For the acquisition of precise images, a luminosity sensor located in the upper part of the UAV was used. The flight plan was designed with a 75% overlap between images. On the other hand, for the georeferencing of the images, seven ground control points (GCPs) were used, which were measured using a high-precision GNSS and marked with topographic targets [33].

Figure 2. Equipment used in data collection. UAV and radio control, and Parrot Sequoia camera.

2.3. Vegetation Indices Estimation

The multispectral images were acquired using Pix4D Capture (flight plan management). Subsequently, images were georeferenced and brightness was corrected using radiometric calibration and correction in Pix4Dmapper (V4.5.6, Pix4D S.A., Prilly, Switzerland), generating the orthomosaic [25]. The radiometric correction improved the quality of the images since it considered the illumination of the scene and the influence of the sensor. It was executed in three steps: (1) point cloud creation, (2) digital surface map (DSM) and (3) orthomosaic creation to calculate the VIs [34,35]. The resulting multispectral image was RGB (visible) in TIFF format with a high resolution of 2.1 cm/pixel. The VIs were estimated within the area of maize canopy cover that was previously extracted using spatial mask extraction processing in ArcGIS 10.5 software. Table 1 shows the indices evaluated during the five study dates.

Table 1. Vegetation indices applied for maize yield evaluation.

Indices	Equation	Source
Normalized Difference Vegetation Index (NDVI)	$NDVI = \frac{NIR-Red}{NIR+Red}$	[36]
Green Normalized Difference Vegetation Index (GNDVI)	$GNDVI = \frac{NIR-Green}{NIR+Green}$	[37]
Green Chlorophyll Index (GCI)	$GCI = \frac{NIR}{Green} - 1$	[38]
Ratio Vegetation Index (RVI)	$RVI = \frac{NIR}{Red}$	[39]
Normalized Difference RedEdge Index (NDRE)	$NDRE = \frac{NIR-Rededge}{NIR+Rededge}$	[40]
ChlorophyII Index-RedEdge (CIRE)	$CIRE = \frac{NIR}{Rededge} - 1$	[38]
ChlorophyII Vegetation Index (CVI)	$CVI = \frac{NIR*Red}{Green^2}$	[41]
Modified Chlorophyll Absorption Reflectance Index (MCARI)	$MACARI = \frac{[(Rededge-Red)-0.2\ (Rededge-Green)]*\left(\frac{Rededge}{Red}\right)}{\frac{(1+0.16)*(Rededge-Red)}{Rededge+Red+0.16}}$	[42]
Soil Adjusted Vegetation Index (SAVI)	$SAVI = \frac{(NIR-Red)(1+L)}{NIR+Red+L}$	[43]
Canopy Chlorophyll Content Index (CCCI)	$CCCI = \frac{\frac{NIR-Rededge}{NIR+Rededge}}{\frac{NIR-Red}{NIR+Red}}$	[44]

2.4. Canopy Cover Estimation

The calculation of the canopy cover was made using the image classification, editor and spatial analysis tools (Spatial Analyst Tools) of the ArcMap software (ArcGIS 10.4.1). Supervised classification of the mosaics was carried out in three classes (vegetable cover, soil and shade) [34], obtained in Section 2.3, which allowed determining the maize cover [34]. From these, an output surface map with plant cover was generated, which allowed the calculating of the percentages of maize cover from the orthomosaics generated for each date.

2.5. Data Analysis and Model Development

Firstly, agronomical yield measurement for each maize hybrid was estimated based on the weights of dry grain of maize expressed in t/ha. The canopy cover and VIs were estimated from the multispectral images at 31, 39, 42, 46 and 51 DAS. An analysis of variance (ANOVA) and Duncan test (alpha = 0.05) means comparisons were performed among maize hybrids on each date evaluated. With the data over time, box plot graphs were constructed over the five dates for each variable evaluated in the experiment to observe the variability. We conducted a Principal Component Analysis (PCA) with R libraries *factoMineR* [45], *factoextra* [46], and *ggplot2* [47] to determine the most relevant index in predicting yield and the variations between each VIs over time. Subsequently, the r-Pearson correlation was applied to the indices with greater performance precision using *GGally* [48] and *Hmisc* [49] libraries. Finally, the yield means between the four maize varieties were compared using Duncan's test with con α = 0.05, using the *agricolae* [50] library. These analyzes were performed with the programming software R [51].

3. Results

3.1. Yield for Each Maize Hybrid and Canopy Cover Estimation

Figure S1 shows the results of applying the Duncan test to compare the means of yield per hybrid and the percentage of canopy cover, according to DAS and VIs. Two groups without significant differences were identified, the first consisting of Advanta9313 (9.91 $\pm$ 2.15 t/ha) and Dekalb7508 (8.85 $\pm$ 1.38 t/ha), and the second MH_INIA619 (6.23 $\pm$ 1.51 t/ha) and Exp_05MLM (5.81 $\pm$ 1.21 t/ha) (Figure S1a). The yield varies from 5.81 to 9.91 t/ha. The hybrids Advanta9313 and Decalb7508 presented the highest yield and the hybrid Exp_05MLM reported the lowest (Figure S1b). At the level of canopy coverage at 31 DAS, the hybrid Exp_05MLM presented greater coverage, followed by Dekalb7508 and MH_INIA619. Dekalb7508 presented greater canopy coverage at 39 and 46 DAS. However, at 51 DAS the canopy cover for the four hybrids was similar.

3.2. Vegetation Indices Estimations and Canopy Cover Relationships

The canopy cover according to the DAS is shown in Figure 3a. Greater variability of canopy cover at 31 DAS is depicted, which improved at 51 DAS. The correlation between the VIs with the DAS (Figure 3b–k) indicated that the reflectance values for nine indices increased continuously. Only the MCARI reported a decrease at 42 DAS. The GNDVI, GCI, RVI, NDRE, CIRE and CCCI indices showed the high significance of plant cover at 46 DAS and the GNDVI, GCI, NDRE, CIRE, CVI, MCARI and CCCI indices at 51 DAS.
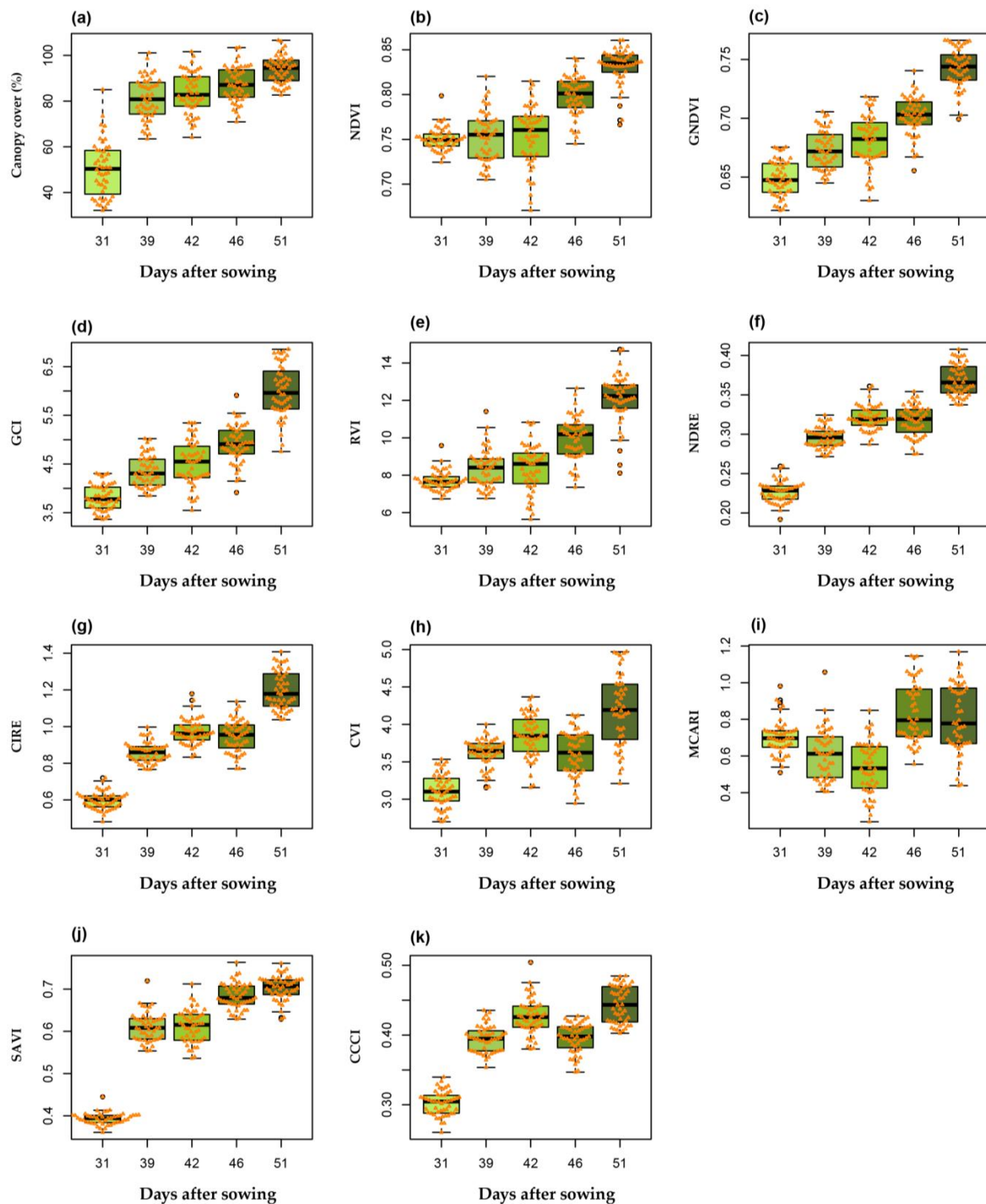
Figure 3. Comparison of canopy cover according to DAS and vegetation indices: (**a**) Canopy cover; (**b**) NDVI; (**c**) GNDVI, (**d**) GCI; (**e**) RVI, (**f**) NDRE; (**g**) CIRE, (**h**) CVI; (**i**) MCARI; (**j**) SAVI; (**k**) CCCI.

3.3. Development of Prediction Models to Calculate Crop Yields

Figure 4 shows the r-Pearson correlation between DAS, crop yield, canopy cover and VIs. The highest correlation between crop yield and canopy cover occurs at 39 and 51 DAS with −0.41 ** and −0.43 **, respectively. At the level of VIs and performance with directly proportional correlations, the GNDVI (0.42 **) and GCI (0.41 **) indices presented correlations of medium importance. The NDRE (0.58 ***), CIRE (0.57 ***) and CCCI (0.54 ***) indices reported a highly significant correlation at 46 DAS (Figure 4d). Likewise, at 51 DAS, the GNDVI (0.55 ***), GCI (0.57 ***), NDRE (0.78 ***), CIRE (0.78 ***), CVI (0.52 ***) and CCCI (0.64 ***) indices showed

a very significant correlation. On the other hand, inversely proportional correlations of crop yield with VI show SAVI (-0.32 *) and MACARI (-0.36 *) at 31 and 51 DAS (Figure 4e).
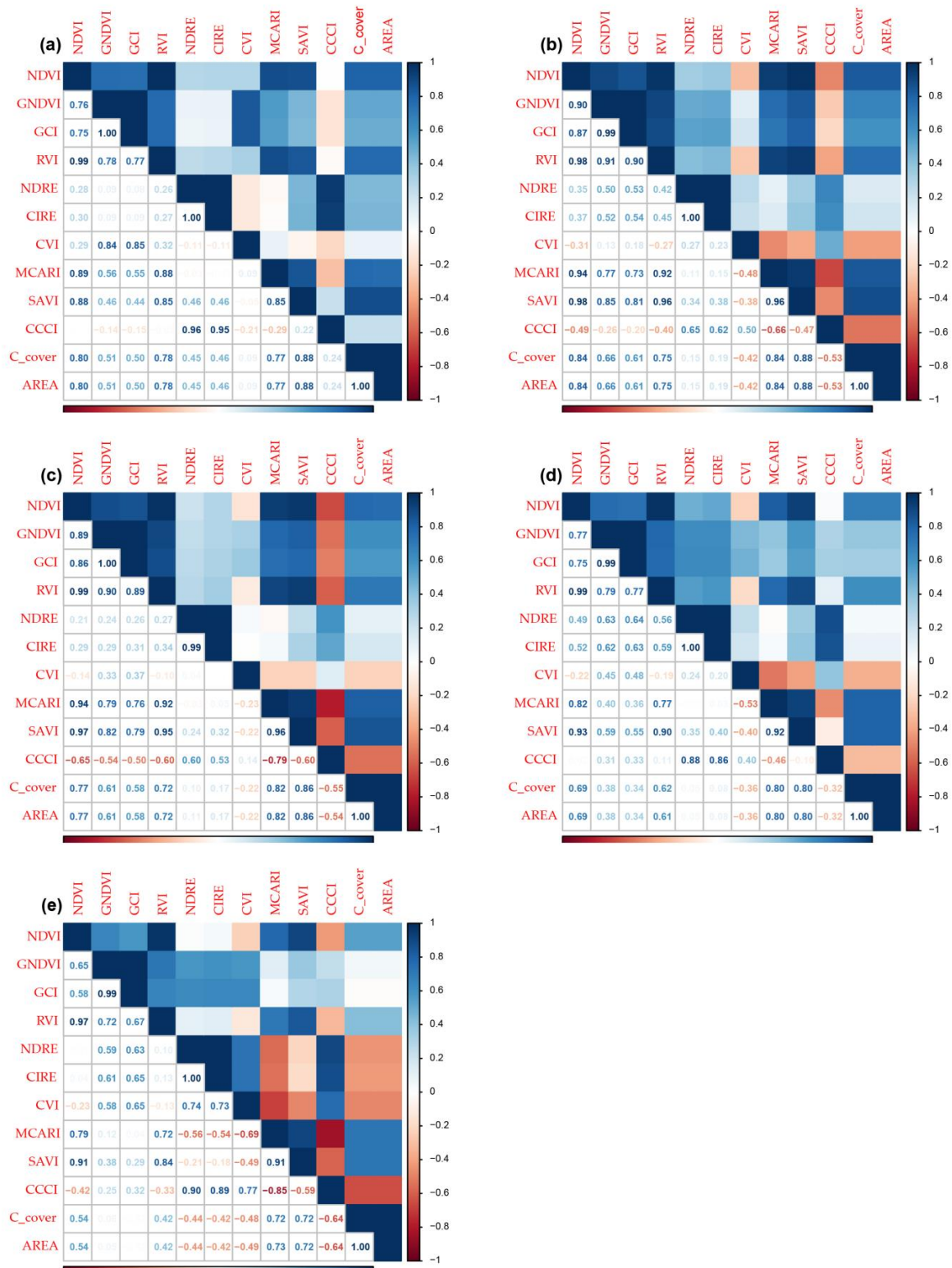

Figure 4. r-Pearson correlation between maize yield with canopy cover and vegetation indices: (**a**) 31 DAS; (**b**) 39 DAS; (**c**) 42 DAS, (**d**) 46 DAS; (**e**) 51 DAS.

The relationship between canopy cover and VIs is shown. The NDVI, MCARI and SAVI indices reported highly significant correlations for all evaluation days, obtaining

the maximum values (0.84 ***, 0.84 *** and 0.88 ***, respectively) at 39 DAS. In turn, the correlation for the GNDVI, GCI, and RVI indices at 51 DAS varies from very significant to medium importance. However, for the CVI and CCCI indices, the inverse correlation increases according to the DAS.

The results of the PCA are presented in Figure 5 for the five dates evaluated. There is a variability of the VI according to the temporality; the greater the distance from the calculation, the greater the difference between them. For comparison, on days 31, 39 and 51 DAS, there is no group overlap (Figure 5a), indicating clear discrimination of the groups in this multivariate analysis. However, the opposite occurs at 39, 42 and 46 DAS, where there is an overlap because they are very close dates that do not allow clear discrimination of the indices generated on the maize plant cover.
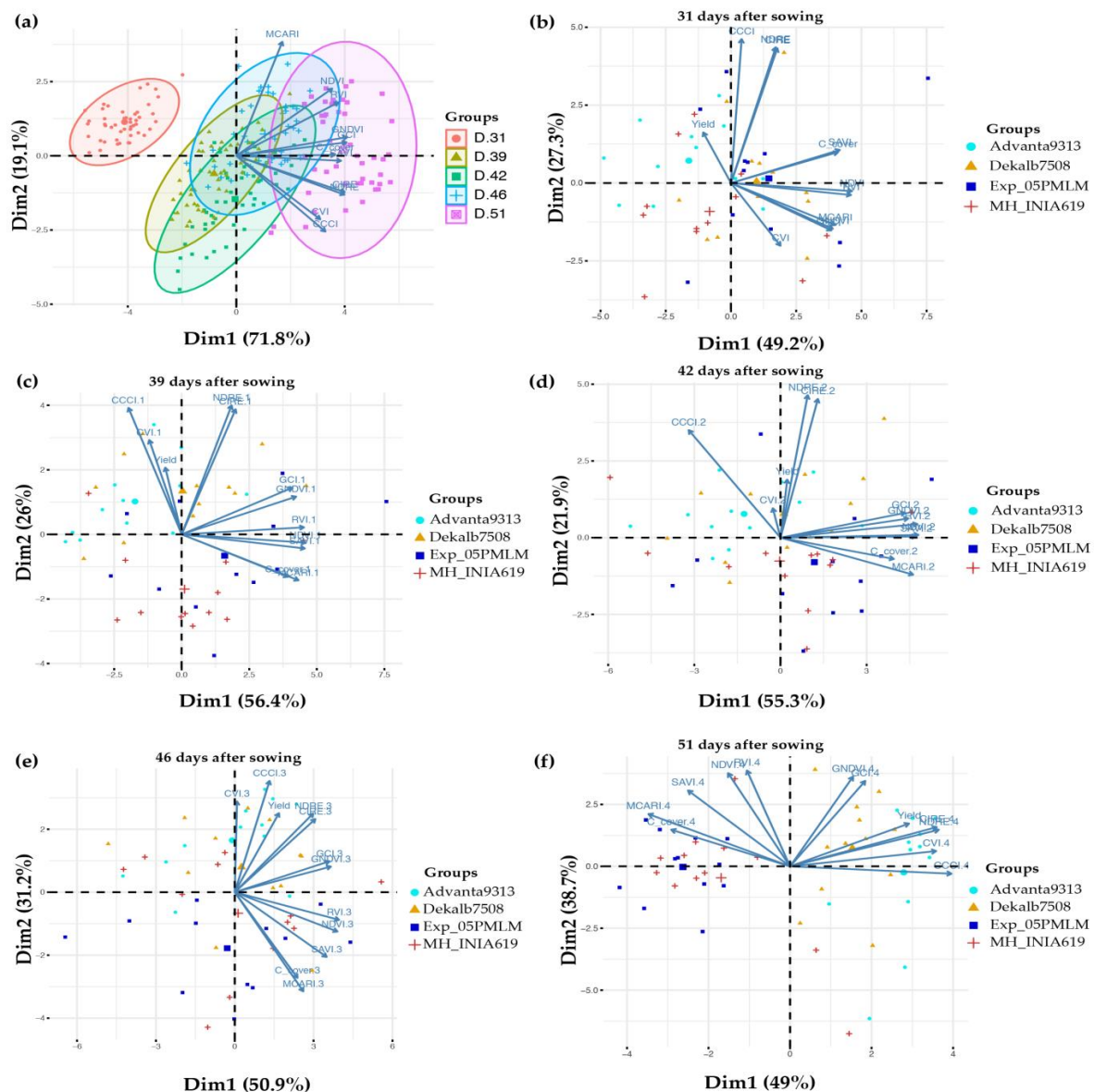
Figure 5. PCA for VIs during the evaluation days: (**a**) PCA for all VIs and DAS; (**b**) PCA for the indices and group of hybrids at 31 DAS; (**c**) PCA for the indices and group of hybrids at 39 DAS; (**d**) PCA for the indices and group of hybrids at 42 DAS; (**e**) PCA for the indices and group of hybrids at 46 DAS; (**f**) PCA for the indices and group of hybrids at 51 DAS.

When performing the PCA for the canopy cover and yield indices at each date of the generated images (Figure 5b–e), we observe that there is no clear discrimination of groups

with respect to the maize hybrids evaluated, but at 51 DAS (Figure 5f) two groups are observed. The maize yield at 51 DAS goes in the same direction as most VIs.

　　Prediction models were built using multiple linear regression based on indices that presented significant correlations with a Pearson's $r > 0.54$ (NDRE, CIRE and CCCI) (Figure 5). Two crop yield prediction models were built for 46 and 51 DAS. Models 1 and 2 were built based on the NDRE, CIRE and CCCI indices at 46 and 51 DAS (Figure 6). Model 1 reported a positive relationship between yield and indices with a coefficient of determination (R^2) of 0.34 (Figure 6a). At the indices level, these values decrease (Figure 6b–d) except for the NDRE which is the highest $R^2 = 0.34$. Model 2 presented a positive relationship with an R^2 of 0.62, higher than model 1. Likewise, at the indices level, NDRE and CIRE presented a highly positive relationship with R^2 0.61 (Figure 6g,h).
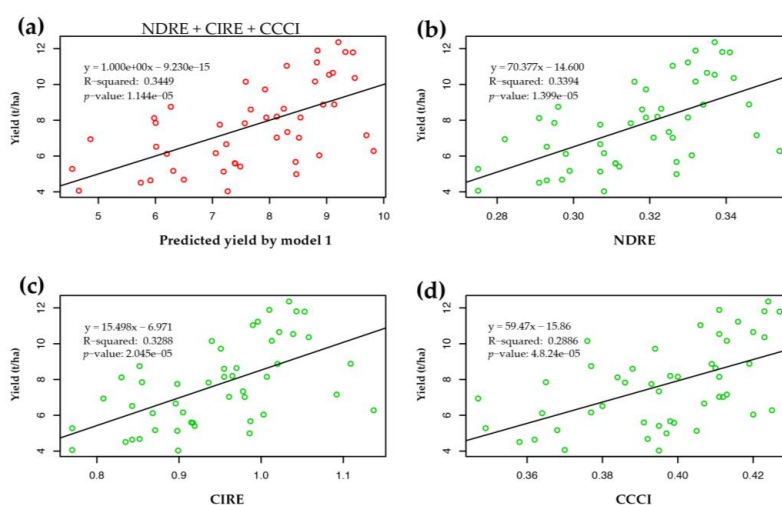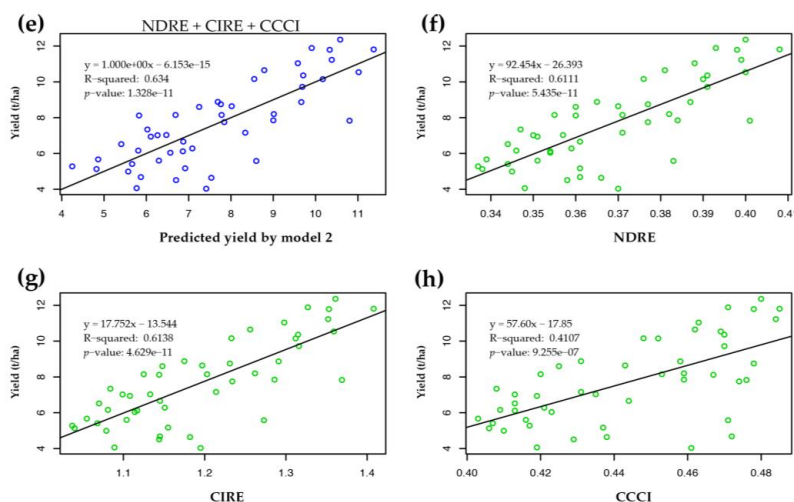
Figure 6. Maize yield prediction models with multiple linear regression: (**a**) Model 1 for performance prediction using the NDRE, CIRE and CCCI indices at 46 DAS; (**b**) Model 1 for performance prediction using NDRE at 46 DAS; (**c**) Model 1 for performance prediction using CIRE at 46 DAS; (**d**) Model 1 for performance prediction using CCCI at 46 DAS; (**e**) Model 2 for performance prediction using the GCI, NDRE and CIRE indices at 51 DAS; (**f**) Model 2 for performance prediction using GCI at 51 DAS; (**g**) Model 2 for performance prediction using NDRE at 51 DAS; (**h**) Model 2 for performance prediction using CIRE at 51 DAS.

4. Discussion

This study predicted maize grain yield for phenological stages using VIs, obtained from UAV multispectral images. One of the advantages of using UAVs in the monitoring of experimental plots or crops is that they can be controlled remotely and generates lower maintenance costs and acquisition of high-resolution images [52]. Hybrid Advanta9313 presented the highest yield (9.91 t/ha) at 51 DAS, a value higher than the national average of 4.77 t/ha [53] and similar to those reported by Gavilánez-Luna & Gómez-Vargas [54]. This superiority in yield performance could be due to its wide adaptability to the maize areas of Peru and its good production stability [55].

For the estimation of canopy cover in the experimental plot, a total of 10 VIs were selected (Table 1). VIs were calculated using multispectral reflectance measurements at visible and near-infrared wavelengths. This range of lengths has been used in different precision agriculture applications such as plant counting, growth monitoring, phenology and chlorophyll measurement. [24,31,52,56,57]. At the VIs level, it is observed that at 46 and 51 DAS, there are highly significant correlations, since, at this stage, the chlorophyll content also increases significantly, as does the canopy cover. In nine indices, values increased cumulatively with the advancing growing season. Only the MCARI showed a decrease at 42 DAS. The NDVI values ranged from 0.75 to 0.83 throughout the evaluation, unlike the GNDVI that went from 0.65 to 0.75, the SAVI being very similar to the NDVI on the first date evaluated. The average values were 0.4 and for the 51 DAS, they oscillated around 0.70.

The models for maize grain yield predictions were based on indices obtained from UAV multispectral images measured on five dates. They were generated from linear regression, demonstrating the feasibility of maize yield prediction using only VIs. In this way, applying metrics through the Pearson correlation helps to determine the most suitable indices to build the prediction models [58]. The feasibility of performance explained by the models ranged between $R^2 = 0.34$ and 0.64 for the 46 and 51 DAS, respectively. The best regression for grain prediction ($R^2 = 0.64$) was obtained with a combination of three indices (NDRE, CIRE and CCCI) at 51 DAS in the flowering stage. Indices NDRE and CIRE presented the highest R^2 (0.61) with the following models: $92.454 \times$ NDRE-26.393 and $17.752 \times$ CIRE-3.544. On the other hand, the R^2 values are lower than those obtained by Barzin et al. [59], who used the index OSAVI y SCCCI. At the same time, Sunoj et al. [60] used exponential and nonlinear NDVI models for yield prediction and obtained R^2 values greater than 0.90. The lower correlations in the early stage may be due to the fact that the physiological characteristics of maize do not yet show significant differences. In other studies, they used satellite images such as MODIS and Landsat 8, where they found high performance predictions at 65–75 and 60–62 DAS, respectively [5,26].

The NDVI showed a low correlation (0.15) for yield estimation. However, higher NDVI values (0.53) have been reported in other studies. This may be due to the location and range of the electromagnetic spectrum taken by the Parrot Sequoia camera [27]. These results are also different from those obtained in wheat crops where the NDVI values fluctuated from 0.40, 0.49 and 0.45, for the early, intermediate and late grain-filling stages for full irrigation treatment [61]. In another study carried out with Landsat images, the indices that best-predicted maize crop yield were Enhanced Vegetation Index (EVI), SAVI and Optimized Soil-Adjusted Vegetation Index (OSAVI), which were different from the NDVI [62]. Through the use of Landsat-7 ETM+ and Spot 5 images, they found high correlation values of the NDVI index in the yield of sugarcane, sugar and barley [63,64].

The approach presented in this study can be implemented with different data sets for different crops. The main advantage of this procedure is that it allowed estimating maize yield with high precision, using IVs calculated from UAVs multispectral images. Furthermore, UAVs and multispectral cameras can provide substantial spatial data on crop yield and quality at a low cost [65]. In addition, they provided the opportunity to monitor farmers' plots, supporting the management of the agricultural system and assisting in decision-making actions.

5. Conclusions

The use of multispectral sensors assembled in the UAV can generate VIs measurements that allowed us to compare the performance of maize hybrids. The results indicated a highly significant correlation between canopy cover and 10 VIs derived from UAV multispectral images. The performance showed high correlations at 46 DAS with six indices (GNDVI, GCI, RVI, NDRE, CIRE and CCCI) and at 51 DAS with seven indices (GNDVI, GCI, NDRE, CIRE, CVI, MCARI and CCCI). Prediction models for performance from multiple correlations at 46 and 51 DAS were similar when three indices or just one were used. The PCA indicated clear discrimination of the dates evaluated with the VIs at 31, 39 and 51 DAS. The maize hybrids Dekalb7508 and Advanta9313 presented better performance than MH_INIA619 and Exp_05PMLM. Maize yield showed a high correlation during the reproductive stage (46 and 51 DAS) with the indices (GNDVI, GCI, RVI, NDRE, CIRE, CVI, MCARI and CCCI). Consequently, when compared to manual evaluation, VIs will allow timely decisions to be made when monitoring maize crops, optimizing resources and helping in making timely decisions in agriculture.

References

1. Naciones Unidas. Paz, Dignidad e Igualdad en un Planeta Sano. *Una Población en Crecimiento.* Available online: https://www.un.org/es/sections/issues-depth/population/index.html (accessed on 18 April 2022).
2. Obour, P.B.; Arthur, I.K.; Owusu, K. The 2020 Maize Production Failure in Ghana: A Case Study of Ejura-Sekyedumase Municipality. *Sustainability* **2022**, *14*, 3514. [CrossRef]
3. Zhao, M.; Bingcan, C. Maize Oil. *Ref. Modul. Food Sci.* **2022**, 22. [CrossRef]
4. FAO. Nota Informativa de la FAO Sobre la Oferta y la Demanda de Cereales. Available online: https://www.fao.org/worldfoodsituation/csdb/es/ (accessed on 10 April 2022).
5. Ahmad, A.; Ordoñez, J.; Cartujo, P.; Martos, V. Remotely piloted aircraft (RPA) in agriculture: A pursuit of sustainability. *Agronomy* **2020**, *11*, 7. [CrossRef]
6. Carrer, M.J.; de Souza Filho, H.M.; Vinholis, M.d.M.B.; Mozambani, C.I. Precision agriculture adoption and technical efficiency: An analysis of sugarcane farms in Brazil. *Technol. Forecast. Soc. Change* **2022**, *177*, 121510. [CrossRef]
7. Manlove, J.L.; Shew, A.M.; Obembe, O.S. Arkansas producers value upload speed more than download speed for precision agriculture applications. *Comput. Electron. Agric.* **2021**, *190*, 106432. [CrossRef]
8. Erickson, B.; Fausti, S.W. The role of precision agriculture in food security. *Agron. J.* **2021**, *113*, 4455–4462. [CrossRef]

9. Urbahs, A.; Jonaite, I. Features of the use of unmanned aerial vehicles for agriculture applications. *Aviation* **2013**, *17*, 170–175. [CrossRef]
10. Tey, Y.S.; Brindal, M. Factors influencing the adoption of precision agricultural technologies: A review for policy implications. *Precis. Agric.* **2012**, *13*, 713–730. [CrossRef]
11. Haghverdi, A.; Washington-Allen, R.A.; Leib, B.G. Prediction of cotton lint yield from phenology of crop indices using artificial neural networks. *Comput. Electron. Agric.* **2018**, *152*, 186–197. [CrossRef]
12. Wu, G.; Miller, N.D.; de Leon, N.; Kaeppler, S.M.; Spalding, E.P. Predicting *Zea Mays* flowering time, yield, and kernel dimensions by analyzing aerial images. *Front. Plant Sci.* **2019**, *10*, 1251. [CrossRef]
13. Danilevicz, M.F.; Bayer, P.E.; Boussaid, F.; Bennamoun, M.; Edwards, D. Maize yield prediction at an early developmental stage using multispectral images and genotype data for preliminary hybrid selection. *Remote Sens.* **2021**, *13*, 3976. [CrossRef]
14. Wulder, M.A.; Masek, J.G.; Cohen, W.B.; Loveland, T.R.; Woodcock, C.E. Opening the archive: How free data has enabled the science and monitoring promise of Landsat. *Remote Sens. Environ.* **2012**, *122*, 2–10. [CrossRef]
15. Guo, W.; Maas, S.J.; Bronson, K.F. Relationship between cotton yield and soil electrical conductivity, topography, and Landsat imagery. *Precis. Agric.* **2012**, *13*, 678–692. [CrossRef]
16. Soriano-González, J.; Angelats, E.; Martínez-Eixarch, M.; Alcaraz, C. Monitoring rice crop and yield estimation with Sentinel-2 data. *Field Crop. Res.* **2022**, *281*, 108507. [CrossRef]
17. Marshall, M.; Belgiu, M.; Boschetti, M.; Pepe, M.; Stein, A.; Nelson, A. Field-level crop yield estimation with PRISMA and Sentinel-2. *ISPRS J. Photogramm. Remote Sens.* **2022**, *187*, 191–210. [CrossRef]
18. Han-Ya, I.; Ishii, K.; Noguchi, N. Satellite and aerial remote sensing for production estimates and crop assessment. *Environ. Control Biol.* **2010**, *48*, 51–58. [CrossRef]
19. Rani, A.; Chaudhary, A.; Sinha, N.K.; Mohanty, M.; Chaudhary, R.S. Drone: The green technology for future agriculture. *Soil Helath Technol. Interv.* **2019**, *2*, 3–6.
20. Du, M.; Noguchi, N. Monitoring of wheat growth status and mapping of wheat yield's within-field spatial variations using color images acquired from UAV-camera system. *Remote Sens.* **2017**, *9*, 289. [CrossRef]
21. Deery, D.; Jimenez-Berni, J.; Jones, H.; Sirault, X.; Furbank, R. Proximal Remote Sensing Buggies and Potential Applications for Field-Based Phenotyping. *Agronomy* **2014**, *4*, 349–379. [CrossRef]
22. Montes, J.M.; Technow, F.; Dhillon, B.S.; Mauch, F. High-throughput non-destructive biomass determination during early plant development in maize under field conditions. *Field Crop. Res.* **2011**, *121*, 268–273. [CrossRef]
23. Pölönen, I.; Saari, H.; Kaivosoja, J.; Honkavaara, E.; Pesonen, L. Hyperspectral imaging based biomass and nitrogen content estimations from light-weight UAV. *Remote Sens. Agric. Ecosyst. Hydrol. XV* **2013**, *8887*, 88870J. [CrossRef]
24. Pino, E.V. Los drones una herramienta para una agricultura eficiente: Un futuro de alta tecnología. *Idesia (Arica)* **2019**, *37*, 75–85. [CrossRef]
25. Zaigham, S.M.; Awais, M.; Khan, F.S.; Afzal, U.; Naz, N.; Khan, M.I. Unmanned air vehicle based high resolution imagery for chlorophyll estimation using spectrally modified vegetation indices in vertical hierarchy of citrus grove. *Remote Sens. Appl. Soc. Environ.* **2021**, *23*, 100596. [CrossRef]
26. Bolton, D.K.; Friedl, M.A. Forecasting crop yield using remotely sensed vegetation indices and crop phenology metrics. *Agric. For. Meteorol.* **2013**, *173*, 74–84. [CrossRef]
27. Ihuoma, S.O.; Madramootoo, C.A. Crop reflectance indices for mapping water stress in greenhouse grown bell pepper. *Agric. Water Manag.* **2019**, *219*, 49–58. [CrossRef]
28. Gong, Y.; Duan, B.; Fang, S.; Zhu, R.; Wu, X.; Ma, Y.; Peng, Y. Remote estimation of rapeseed yield with unmanned aerial vehicle (UAV) imaging and spectral mixture analysis. *Plant Methods* **2018**, *14*, 70. [CrossRef] [PubMed]
29. Ahmed, I.; ur Rahman, M.H.; Ahmed, S.; Hussain, J.; Ullah, A.; Judge, J. Assessing the impact of climate variability on maize using simulation modeling under semi-arid environment of Punjab, Pakistan. *Environ. Sci. Pollut. Res.* **2018**, *25*, 28413–28430. [CrossRef]
30. da Silva, E.E.; Rojo Baio, F.H.; Ribeiro Teodoro, L.P.; da Silva Junior, C.A.; Borges, R.S.; Teodoro, P.E. UAV-Multispectral and vegetation indices in soybean grain yield prediction based on in situ observation. *Remote Sens. Appl. Soc. Environ.* **2020**, *18*, 100318. [CrossRef]
31. Guo, Y.; Chen, S.; Li, X.; Cunha, M.; Jayavelu, S.; Cammarano, D.; Fu, Y. Machine Learning-Based Approaches for Predicting SPAD Values of Maize Using Multi-Spectral Images. *Remote Sens.* **2022**, *15*, 1337. [CrossRef]
32. López-Calderón, M.J.; Estrada-ávalos, J.; Rodríguez-Moreno, V.M.; Mauricio-Ruvalcaba, J.E.; Martínez-Sifuentes, A.R.; Delgado-Ramírez, G.; Miguel-Valle, E. Estimation of total nitrogen content in forage maize (*Zea Mays* L.) Using Spectral Indices: Analysis by Random Forest. *Agriculture* **2020**, *10*, 451. [CrossRef]
33. Fawcett, D.; Panigada, C.; Tagliabue, G.; Boschetti, M.; Celesti, M.; Evdokimov, A.; Biriukova, K.; Colombo, R.; Miglietta, F.; Rascher, U.; et al. Multi-scale evaluation of drone-based multispectral surface reflectance and vegetation indices in operational conditions. *Remote Sens.* **2020**, *12*, 514. [CrossRef]
34. Achicanoy, J.A.; Rojas-Robles, R.; Sánchez, J.E. Análisis y proyección de las coberturas vegetales mediante el uso de sensores remotos y sistemas de información geográfica en la localidad de Suba, Bogotá-Colombia. *Gestión Ambient.* **2018**, *21*, 41–58. [CrossRef]
35. McCluney, W.R. *Introduction to Radiometry and Photometry*, 2nd ed.; Artech House: Norwood, MA, USA, 2014, ISBN 978-1608078332.

36. Peñuelas, J.; Gamon, J.A.; Griffin, K.L.; Field, C.B. Assessing community type, plant biomass, pigment composition, and photosynthetic efficiency of aquatic vegetation from spectral reflectance. *Remote Sens. Environ.* **1993**, *46*, 110–118. [CrossRef]

37. Gitelson, A.A.; Kaufman, Y.J.; Merzlyak, M.N. Use of a green channel in remote sensing of global vegetation from EOS- MODIS. *Remote Sens. Environ.* **1996**, *58*, 289–298. [CrossRef]

38. Gitelson, A.A.; Gritz, Y.; Merzlyak, M.N. Relationships between leaf chlorophyll content and spectral reflectance and algorithms for non-destructive chlorophyll assessment in higher plant leaves. *J. Plant Physiol.* **2003**, *160*, 271–282. [CrossRef]

39. Pearson, R.L.; Miller, L.D. Remote mapping of standing crop biomass for estimation of the productivity of the shortgrass Prairie. *Remote Sens. Environ. VIII* **1972**, *1*, 1355. Available online: https://ui.adsabs.harvard.edu/abs/1972rse..conf.1355P/abstract (accessed on 10 April 2022).

40. Gitelson, A.; Merzlyak, M.N. Quantitative estimation of chlorophyll-a using reflectance spectra: Experiments with autumn chestnut and maple leaves. *J. Photochem. Photobiol. B Biol.* **1994**, *22*, 247–252. [CrossRef]

41. Vincini, M.; Frazzi, E.; D'Alessio, P. A broad-band leaf chlorophyll vegetation index at the canopy scale. *Precis. Agric.* **2008**, *9*, 303–319. [CrossRef]

42. Guan, L.; Liu, X.N.; Cheng, C.Q. Research on hyperspectral information parameters of chlorophyll content of rice leaf in cd-polluted soil environment. *Guang Pu Xue Yu Guang Pu Fen Xi/Spectrosc. Spectr. Anal.* **2009**, *29*, 2713–2716. [CrossRef]

43. Alam, M.J.; Rahman, K.M.; Asna, S.M.; Muazzam, N.; Ahmed, I.; Chowdhury, M.Z. A Soil-Adjusted Vegetation Index (SAVI). *Remote Sens. Environ.* **1988**, *25*, 295–309. [CrossRef]

44. Raper, T.B.; Varco, J.J. Canopy-scale wavelength and vegetative index sensitivities to cotton growth parameters and nitrogen status. *Precis. Agric.* **2015**, *16*, 62–76. [CrossRef]

45. Le, S.; Josse, J.; Huaaon, F. FactoMineR: An R package for multivariate analysis. *J. Stat. Softw.* **2008**, *25*, 1–18. [CrossRef]

46. Kassambara, A.; Mundt, F. Package "Factoextra". Available online: https://cran.r-project.org/web/packages/factoextra/factoextra.pdf (accessed on 12 November 2021).

47. Wickham, H. *ggplot2: Elegant Graphics for Data Analysis*, 2nd ed.; Springer-Verlag: Cham, Switzerland, 2016.

48. Schloerke, B.; Cook, D.; Larmarange, J.; Briatte, F.; Marbach, M.; Thoen, E.; Elberg, A.; Crowley, J. Package "GGally". Available online: https://cran.r-project.org/web/packages/GGally/GGally.pdf (accessed on 12 November 2021).

49. Miscellaneous, T.H.; Yes, L. Package "Hmisc". Available online: https://cran.r-project.org/web/packages/Hmisc/Hmisc.pdf (accessed on 12 November 2021).

50. Package, T.; Mendiburu, A.F. Package "Agricolae". Available online: https://cran.r-project.org/web/packages/agricolae/agricolae.pdf (accessed on 12 November 2021).

51. R Core Team. *R: A Language and Environment for Statistical Computing*; R Foundation for Statistical Computing: Vienna, Austria, 2021; Available online: https://www.r-project.org/ (accessed on 12 November 2021).

52. Pudelko, R.; Stuczynski, T.; Borzecka-Walker, M. The Suitability of an Unmanned Aerial Vehicle (UAV) for the Evaluation of Experimental Fields and Crops. *Zemdirbyste* **2012**, *99*, 431–436.

53. MIDAGRI. Perfil Productivo y Competitivo de los Principales Cultivos del Sector. Available online: https://acortar.link/fjrSc (accessed on 11 April 2021).

54. Gavilánez-Luna, F.C.; Gómez-Vargas, M.J. Definición de dosis de nitrógeno, fósforo y potasio para una máxima producción del maíz híbrido Advanta 9313 mediante el diseño central compuesto. *Cienc. Tecnol. Agropecu.* **2022**, *23*, e2225. [CrossRef]

55. Farmagro. Maíz Adv 9313. Available online: http://www.farmagro.com.pe/p/advanta-9313/ (accessed on 6 April 2022).

56. Jin, X.-L.; Diao, W.-Y.; Xiao, C.-H.; Wang, F.-Y.; Chen, B.; Wang, K.-R.; Li, S.-K. Estimation of Wheat Agronomic Parameters Using New Spectral Indices. *PLoS ONE* **2013**, *8*, e72736. [CrossRef]

57. Gómez-Candón, D.; Virlet, N.; Labbé, S.; Jolivot, A.; Regnard, J.L. Field phenotyping of water stress at tree scale by UAV-sensed imagery: New insights for thermal acquisition and calibration. *Precis. Agric.* **2016**, *17*, 786–800. [CrossRef]

58. Marques, A.P.; Prado, L.; Garcia, D.E.; Nunes, W.; Cordeiro, D.; Ribeiro, L.P.; da Silva Junior, C.A.; Capristo-Silva, G.F.; Li, J.; Rojo, F.H.; et al. A Random Forest Ranking Approach to Predict Yield in Maize with Uav-Based Vegetation Spectral Indices. *Comput. Electron. Agric.* **2020**, *178*, 105791. [CrossRef]

59. Barzin, R.; Pathak, R.; Lotfi, H.; Varco, J.; Bora, G.C. Use of UAS multispectral imagery at different physiological stages for yield prediction and input resource optimization in maize. *Remote Sens.* **2020**, *12*, 2392. [CrossRef]

60. Suno, S.; Cho, J.; Guinness, J.; van Aardt, J.; Czymmek, K.J.; Ketterings, Q.M. Corn grain yield prediction and mapping from Unmanned Aerial System (UAS) multispectral imagery. *Remote Sens.* **2021**, *13*, 3948. [CrossRef]

61. Hassan, M.A.; Yang, M.; Rasheed, A.; Yang, G.; Reynolds, M.; Xia, X.; Xiao, Y.; He, Z. A rapid monitoring of NDVI across the wheat growth cycle for grain yield prediction using a multi-spectral UAV platform. *Plant Sci.* **2019**, *282*, 95–103. [CrossRef] [PubMed]

62. Peroni, L.; Chartuni, E.; do Amaral, C.H.; Usher, C.M.; Zution, I.; Filgueiras, R.; Coelho, F. Potential of using spectral vegetation indices for maize green biomass estimation based on their relationship with the photosynthetic vegetation sub-pixel fraction. *Agric. Water Manag.* **2020**, *236*, 106155. [CrossRef]

63. Zenteno, G.A.; Palacios, E.; Tijerina, L.; Flores, H. Aplicación de tecnologías de percepción remota para la estimación del rendimiento en caña de azúcar. *Rev. Mex. Cienc. Agrícolas* **2017**, *8*, 1575–1586. [CrossRef]

64. Montealegre, F.A. Evaluación Espacio Temporal de la Productividad Agrícola Con Índices de Vegetación de Diferencias Normalizadas (NDVI) Como Herramienta Para el Ordenamiento Territorial. Caso de Estudio Cuenca Alta del Arroyo Napaleofú, Provincia de Buenos Aires, Argentina. M.Sc. Thesis, Universidad Nacional de la Plata-Argentina, La Plata, Argentina, 2017.

65. Zhou, X.; Kono, Y.; Win, A.; Matsui, T.; Tanaka, T.S.T. Predicting within-field variability in grain yield and protein content of winter wheat using UAV-Based multispectral imagery and machine learning approaches. *Plant Prod. Sci.* **2021**, *24*, 137–151. [CrossRef]